ACS OMEGA

http://pubs.acs.org/journal/acsodf

Article

DNA Antiadhesive Layer for Reusable Plasmonic Sensors: Nanostructure Pitch Effect

Remigiusz K. Trojanowicz,[‖] Ambra Vestri,*[,‖] Massimo Rippa, Joseph Zyss, Katarzyna Matczyszyn, and Lucia Petti*

Cite This: *ACS Omega* 2022, 7, 31682−31690

Read Online

ACCESS | Metrics & More | Article Recommendations | Supporting Information

ABSTRACT: A long-term reusable sensor that provides the opportunity to easily regenerate the active surface and minimize the occurrence of undesired absorption events is an appealing solution that helps to cut down the costs and improve the device performances. Impressive advances have been made in the past years concerning the development of novel cutting-edge sensors, but the reusability can currently represent a challenge. Direct shielding of the sensor surface is not always applicable, because it can impact the device performance. This study reports an antiadhesive layer (AAL) made of 90 mg/mL DNA sodium salt from salmon testes (ssstDNA) for passivating gold plasmonic sensor surfaces. Our gold two-dimensional (2D) nanostructured plasmonic metasurfaces modified with AAL were used for DNA quantification. AAL is thin enough that the plasmonic sensor remains sensitive to subsequent deposition of DNA, which serves as an analyte. AAL protects the gold surface from unwanted nonspecific adsorption by enabling wash-off of the deposited analyte after analysis and thus recovery of the LSPR peak position (rLSPR). The calibration curve obtained on a single nanostructure (Achiral Octupolar, 100 nm pitch) gave an LOD = 105 ng/mL and an extraordinary dynamic range, performances comparable or superior to those of commercial UV−vis spectrometers for acid nucleic dosage. Two different analytes were tested: ssstDNA (~2000 bp) in deionized water and double-strand DNA (dsDNA) of 546−1614 bp in 100 mM Tris buffer and 10 mM $MgCl_2$. The two nanostructures (Achiral Octupolar 25 and 100) were found to have the same sensitivity to DNA in deionized water but different sensitivity to DNA in a salt/buffer solution, opening a potential for solute discrimination. To the best of our knowledge, this is the first report on the use of AAL made of several kilobase-pairs-long dsDNA to produce a reusable plasmonic sensor. The working principle and limitations are drawn based on the LSPR and SERS study.

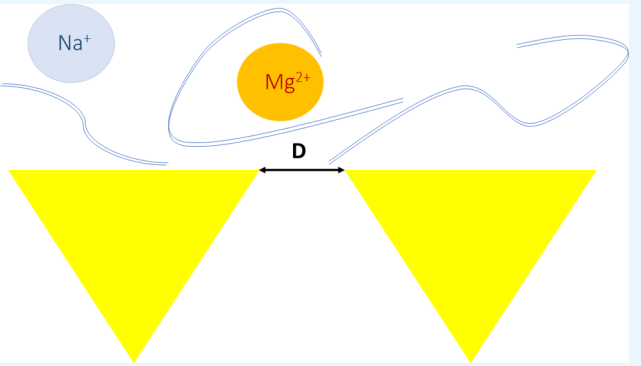

1. INTRODUCTION

Reusability is one of the most desired features of commercially available sensors. Proper regeneration of the sensing surface and the minimization of undesired absorption events can currently represent an important limit for detection purposes, despite the recent impressive advances made in the sensor field, in particular for medical applications.[1,2] Covers or membranes constitute a fundamental construction element preventing damage or cross-talk, but they are not the optimal solution to each case.

High-performance plasmonic sensors have been widely appreciated in the past decades for their versatility and ability to allow label-free, simple, sensitive, fast, and cost-effective analysis, and the recent cutting-edge literature on the subject proves the still vibrant research interest in plasmonic systems for different sensing purposes.[3,4]

Direct shielding of the plasmonic sensor surface is not an effective strategy to limit unwanted absorption and/or favor the reusability. In the specific case of localized surface plasmon resonance (LSPR), the working principle requires a close proximity of the analyte to the metal surface acting as a transducing element. The analyte at a few-nanometers distance from the plasmonic area causes refractive index (RI) variations detectable by evaluating the red shift of the plasmonic absorption peak. Clearly, the RI variation is not specifically related to the presence of the analyte of interest; anyway, the specificity of the detection can be simply achieved by immobilizing receptors on the metal surface, which allows the exclusive capture of the target analyte.[5−7]

Inspired by popular protein antiadsorption layers on metal oxides made of PLL-g-PEG,[8,9] we chose a DNA sodium salt

Received: March 7, 2022
Accepted: May 12, 2022
Published: August 30, 2022

https://doi.org/10.1021/acsomega.2c01370
ACS Omega 2022, 7, 31682−31690

from salmon testes (ssstDNA) as a protective antiadhesive layer (AAL) for gold plasmonic sensing surfaces. It serves as a very thin separation between the analyte and the sensor surface and thus maintains the sensitivity of the plasmonic sensor. The performances of the proposed AAL have been here tested by exploiting a gold two-dimensional (2D) nanostructured plasmonic metasurface for nucleic acid quantitation. The monolayer of adsorbed DNA prevents further nonspecific adsorption of subsequent DNA deposition, as already suggested in the review on the physicochemical properties governing the process of DNA adsorption onto gold by Liu.[10] DNA interaction with gold and itself depends on many factors.[11] In particular, gold-dsDNA interaction is relatively much stronger in low-ionic-strength solution, as dsDNA molecules repel each other due to negatively charged phosphate backbones.[11] Any kind of physisorption between adjacent double-strand DNA (dsDNA) molecules in the dried state is readily broken upon dissolving in water. The monolayer of dsDNA adsorbed onto the sensor surface (ALL) prevents further unwanted adsorption of other DNA molecules.

The plasmonic properties of nanoscale systems and their sensing performance are jointly determined by physicochemical factors such as dielectric properties and the material composition as much as geometric factors. For this reason, the shape, size, period, and symmetry of the engineered plasmonic nanostructure are designed to obtain enhanced field distribution at the desired wavelength[12] or even the effective sensing volume available for a particular analyte.[13−15] Over the years, our team had also empirically observed that some patterns of specific pitches provide superior performance for a particular analyte, and so we have developed LSPR- and SERS-based sensors of molecules, biomacromolecules, and viruses, e.g., Thiram pesticide on Thue-Morse arranged triangular nanopillars,[16] bovine serum albumin and imidacloprid insecticide on iso-Y-shaped nanopillars,[17,18] rotavirus on Achiral Octupolar arranged triangular nanopillars,[19] and hepatitis A on pyramidal nanoholes.[20] In this study, we explore the functionality and limitations of AAL on a 2D plasmonic photonic crystal−glass/ITO substrate with gold triangular pillars arranged in Achiral Octupolar pattern with a pitch of 25, 50, 100, and 263 nm (AchOct 25/50/100/263). In this regard, it has been shown that nanostructures based on unit cells with octupolar tensor symmetry, such as inspired by trigonal and tetrahedral molecules, allow for highly sensitive plasmonic devices.[21,22] Our nanopattern dimensions were chosen to be in the order of magnitude of persistence length (40−120 nm salt dependent[23]) and gyration radius of dsDNA (213 nm for linear 5.9 kbp[24]).

In this work we test the performances of our plasmonic chip passivated with AAL, exploring the possibility of total nucleic acid quantification. The calibration curve obtained by exploiting the AchOct 100 metasurface was characterized by an LOD = 105 ng/mL and an extraordinary dynamic range, performances comparable or superior to those of commercial UV−vis spectrometers for acid nucleic dosage.[25] Moreover, our reusable chips allow a sensitive detection without the need for labeling or complex sample procedures as required for other methods commonly used for DNA quantitation, such as fluorescence-based assays.[26]

We also attempt to investigate the influence of the acid nucleic size and the sample medium composition on the sensor response by using DNA of different molecular weights in deionized water, in a 100 mM Tris buffer and 10 mM $MgCl_2$ salt solution.

It is important to note that the main purpose of this work is to verify the suitability of our AAL for sensing purposes, and for this reason we chose to perform a simple DNA quantification, as proof-of-concept application. Specific sequence detection is a different goal already achieved by plasmonic devices, as proved in the literature by different works.[27] In this case, the immobilization of RNA, single-strand DNA, or DNA mimic as probes onto the plasmonic surface allows the detection of complementary sequences by annealing. The mentioned approach aims to propose novel biosensors as a remarkable alternative to conventional nucleic acid analysis commonly used to detect specific DNA/RNA sequences of interest, such as real-time PCR.

To the best of our knowledge, we are the first ones to report the use of several thousand kilobase-pair-long dsDNA as a protective shielding for DNA quantitation by LSPR. Moreover, we believe that AAL applicability could be extended to other kinds of LSPR sensor systems, and it would be interesting to investigate its suitability for the development of reusable biosensors capable of specific detection, in the near future.

2. MATERIALS AND METHODS

2.1. Materials. DNA sodium salt from salmon testes (ssstDNA) was bought from Sigma Aldrich, heterogenous distribution ∼2000 bp.[28] The dsDNA of specific molecular weight (PCR DNA: 546, 1064, and 1614 bp; 100 mM Tris 10 mM $MgCl_2$) was self-prepared and checked with Agilent DNA 7500 Assay using the Agilent 2100 Bioanalyzer system—full documentation available online (file PCR_DNA.pdf).

2.2. Fabrication. Nanostructured Au substrates were fabricated by following a procedure identical to the one already described.[19] Briefly, 300 μm × 300 μm Au nanostructures were fabricated by a high-resolution electron beam lithography (EBL) system (Raith 150 EBL system), using a 78 nm layer of styrene methyl acrylate (ZEP 520A) as positive resist. The resist was spin-coated on 2 × 2 cm glass slides covered with a 15 nm indium tin oxide (ITO) conductive layer and baked at 170 °C for 5 min. A 10.2 pA electron beam with an area dose of 27 $\mu C/cm^2$ was used to generate an AchOct pattern consisting of a periodic array of a main unit cell made of 3 big equilateral triangular Au nanostructures with side 170 nm and another smaller inner triangle with side 70 nm. Different minimum interparticle distances between two neighboring unit cells were used to fabricate this kind of structures: 25, 50, 100, and 263 nm. The development of the resist layer after exposure was performed in an n-amyl acetate solvent; then the substrates were incubated for 60 s in 1:3 *N*-ethyl isobutyl ketone:isopropyl alcohol solution (MIBK/IPA) and at last rinsed for 30 s in IPA. At this point, 2 nm Cr and then 50 nm Au were evaporated on the resist surface by a SISTEC CL-400C e-beam system. To achieve the 2D nanopillar structures, the metal bilayer in the nonexposed area was lifted off by soaking the substrates for 3 min in *N*-methyl pyrrolidinone (NMP) at 80 °C, and then IPA was used for rinsing. The realized metastructures were morphologically characterized by scanning electron microscopy (SEM) in order to verify their conformity in shape and size to the designed project.

2.3. Antiadhesive Layer. ssstDNA was added to deionized water to obtain a 90 mg/mL solution, then vortexed and kept in the fridge for several days to dissolve. AAL was

https://doi.org/10.1021/acsomega.2c01370
ACS Omega 2022, 7, 31682−31690

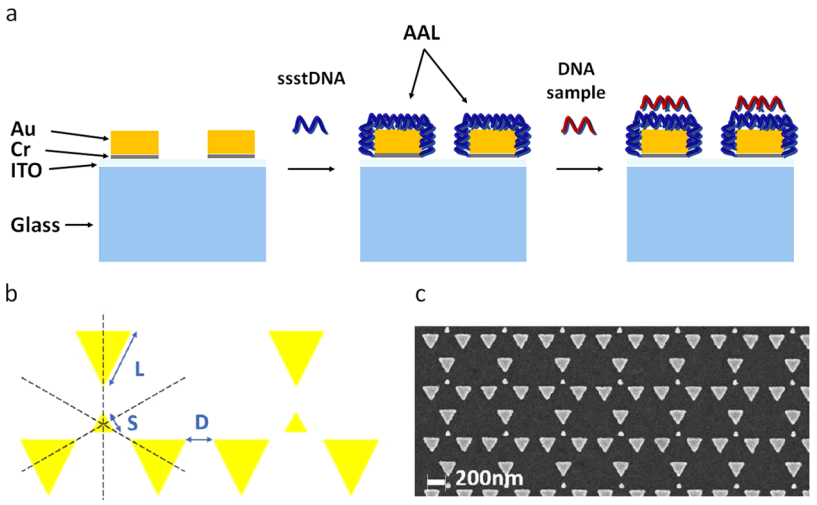

Figure 1. (a) Schematic representation of the sensor chip. Left to right: gold nanopillars on the glass/ITO substrate, passivation with AAL, and DNA sample deposition. (b) Scheme of the achiral octupolar pattern: big prism side I = 170 nm, small prism side S = 70 nm, varied distance between unit cells D = 25/50/100/263 nm. (c) Scanning electron microscopy image of AchOct 100.

done by depositing a 90 mg/mL ssstDNA solution on the chip and leaving it to dry overnight before rinsing the chip with deionized water vigorously. The same procedure was then repeated. The second step was necessary to ensure DNA coverage in case of any defects.

2.4. LSPR Measurements. As previously described,[18] the spectral shifts of the LSPR peaks were measured using an experimental setup consisting of a halogen lamp that provides unpolarized white light to the nanostructured pattern by the use of a 10X (N.A. 0.25) objective (a circular light spot of about 400 μm). The transmission signal was collected by a fiber with a core of 50 μm coupled with a spectrophotometer (Ocean Optics USB4000, optical resolution ~1 nm). The mean extinction spectra were calculated from at least 3 measurements achieved by moving the collection fiber on different areas of the nanostructures, and the LSPR shifts obtained under the different experimental conditions were estimated.

2.5. Calibration Curve. On the Achiral Octupolar 100, we constructed a calibration curve by a 0.5 mL droplet deposition of ssstDNA within the range of 100 ng/mL−90 mg/mL in deionized water onto a chip with the AAL and evaporation in ambient conditions. Subsequently, the LSPR shift was measured. In between each measurement, the chip undergoes a recovery protocol as described below. No degradation of the chip performance was observed when using ssstDNA.

2.6. Recovery Protocol. To recover the LSPR back to its AAL peak position, we simply apply a couple of vigorous rinses with acetone and deionized water to wash off the analyte, leaving only the AAL. After each recovery, the chip is left to dry under a ventilation hood, and LSPR measurement is made, indicating the recovered LSPR peak position (rLSPR).

2.7. PCR DNA and ssstDNA Comparison. Onto a chip passivated with AAL and containing AchOct 25/50/100/263, we drop-cast 0.5 mL of 1 μg/mL ssstDNA and measure the LSPR shift after drying. Then, we follow the recovery protocol in order to measure the rLSPR (3 times). To perform a comparison, we repeat the same procedure using PCR DNA: drop-cast 0.5 mL of PCR DNA, evaporate, measure the LSPR shift, recover and measure the rLSPR, in the following order: 1064, 1614, and 546 bp.

2.8. SERS Measurements. SERS analysis was performed with the Raman system (QE Pro-Raman, Ocean Optics, resolution 4 cm^{-1}) connected to an upright microscope (Olympus BX51) in a backscattering configuration (30−120 s acquisition time, 50× microscope objective with N.A. 0.75, laser wavelength of 785 nm, and power of 12 mW). For the SERS measurements, we perform oxygen plasma cleaning on the Achiral Octupolar 100 chip to remove the AAL and leave the chip bare. Then, we drop-cast, evaporate, and measure the SERS signal of 1 μg/mL ssstDNA that was previously sonicated. Finally, we store the chip (with sonicated ssstDNA) in the fridge in a closed container filled with acetone for 72 h to dehydrate the sonicated ssstDNA.

2.9. Data Analysis. The LOD calculation is described in Suporting Material eq 1. The solutions in mg/mL range create a thick layer on the nanostructure, which lowers the intensity of the light transmitted. It lowers the signal-to-noise ratio and causes potential concerns about thin film interferences. In order to verify this, we performed additional analysis of the Lorentzian fit (Figure S2) and the residuals (Figure S3) for all of the measurements presented on the calibration curve. The full description can be found in the Supporting Material. In short, we show that the LSPR peak position found by using a minimal transmittance and Lorentzian peak fitting differs on average by ±1.1 and ±1.8 nm (for rLSPR and DNA measurements, respectively; Figure S4), which can be disregarded compared to the standard deviation of the measurements.

3. RESULTS AND DISCUSSION

Chips made of glass/ITO substrate with triangular gold nanopillars arranged into the AchOct pattern (2D photonic crystal) and the gold surface passivated with AAL were used to perform LSPR and SERS measurements of the DNA samples (Figure 1a). In the context of nonlinear optics, the term octupolar is related to the 3-fold symmetry and its implication for the quadratic nonlinear susceptibility tensor that is responsible for second harmonic generation. An octupolar pattern can exhibit very interesting optical properties, especially in its interaction with polarized light. Moreover, its rounded-off shape facilitates its packing in a periodic and

https://doi.org/10.1021/acsomega.2c01370
ACS Omega 2022, 7, 31682−31690

compact lattice, as opposed to the less favorable elongated rod-like dipolar molecules.[19,29] The octupolar arrangement was used previously by our team for phage-based SERS detection of pathogens.[22] In this paper, starting from an Achiral Octupolar cell, we have optimized the design by varying the nanostructure pitch (D = 25/50/100/263 nm) within the regime of the DNA hydrodynamic radius and persistence length (both molecular weight dependent). The scheme (Figure 1b) and SEM image (Figure 1c) of the used AchOct structure are presented. The pattern unit cell is composed of a small prism (S = 70 nm) and big prisms (L = 170 nm) spaced by D = 25/50/100/263 nm for AchOct 25/50/100/263, respectively.

We present the following results using a mass concentration rather than a molar concentration, which is readily comparable with other methods—several μg/mL is the typical detection limit for a standard UV−vis spectrophotometer and can be as low as 0.4 μg/mL for Nanodrop 2000c with a 10 mm patch cuvette.[30]

It is important to point out that passivation of the nanostructure with AAL causes a red shift of 18.7, 26.5, 18.1, and 28.1 nm for AchOct 25, AchOct 50, AchOct 100, and AchOct 263, respectively (Figure S1 in Supporting Material). This proves both the presence and the nanoscale thickness of AAL. ssstDNA was chosen due to its optimal molecular weight, commercial availability, and low salt content, and adjusted to the concentration of the DNA liquid-crystal regime.[31] Both the molecular weight and concentration of DNA play an important role in AAL formation; indeed, they influence the packing density, degree of dehydration, and subsequent denaturation upon adsorption onto the surface.

3.1. Calibration Curve and LSPR Regeneration. To verify the performance of AAL, we construct a calibration curve as presented in Figure 2, which gives a logarithmic fit that covers the range from hundreds of ng/mL to several mg/mL. The recovery and evaporation processes are independent of each other. There is some randomness related to the evaporation that should be qualitatively investigated in the well-controlled chamber. For the scope of this study, we simplify the experiment to the standard deviation of the blank samples, rLSPR (σ_{rLSPR} = 2.26 nm; Figure 3), and so was calculated our LOD = 105 ng/mL.

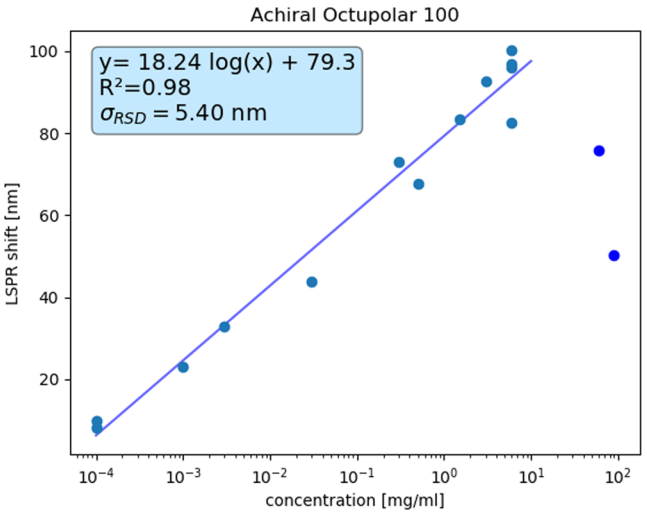

Figure 2. Concentration-dependent LSPR-shift curve of ssstDNA dissolved in deionized water, structure AchOct 100. Parameters of the logarithmic fit in the inset: slope a = 18.24 nm, intercept b = 79.30 nm, determination coefficient R^2 = 0.98, and standard deviation of residuals from the fit σ_{RSD} = 5.40 nm. Fitting only up to 6 mg/mL (limit of the dynamic range).

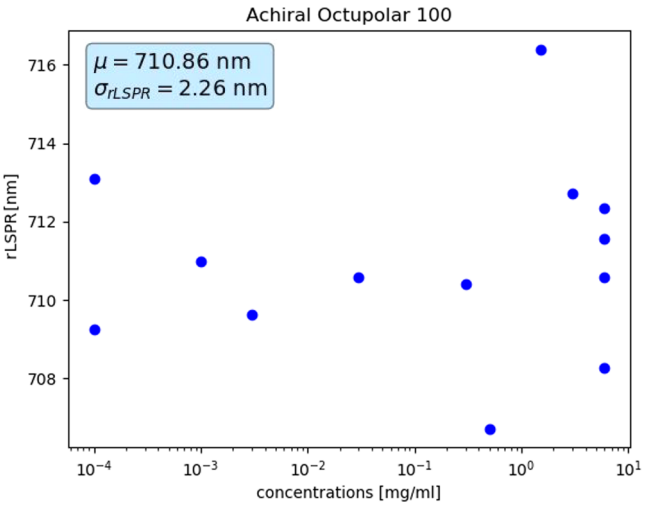

Figure 3. Recovered LSPR (rLSPR) peak after measurement for each concentration used to construct the calibration curve. The mean (μ) and standard deviation (σ) of the rLSPR values are provided in the inset.

Concentrations above several mg/mL upon evaporation form white films that are visible to the naked eye (very viscous solutions) and are known to form liquid-crystal phases.[32] A fit extended over such a range is quite surprising as it would seem that mg/mL solutions should be well above the LSPR sensing volume. Modes in the plasmonic cavities were shown to have a decay length below 5% of the wavelength,[33] while for gratings of 100 nm AuNPs, the calculated characteristic decay length was equal to 22.6 nm.[34] We suspect that it is not simply a matter of thickness of the deposited DNA that causes LSPR shift, but also its packing density within the sensing volume, which must be concentration-dependent, as could be expected from the mentioned concentration-dependent liquid-crystal properties. We also present measurements above saturation, showing the LSPR-shift decline for concentrations of 60 mg/mL (76 nm shift) and 90 mg/mL (51 nm shift). We excluded these DNA concentrations from the fitting, because they clearly deviate from the linear range of our system. For concentrations of tens of mg/mL, the drying process is very slow—overnight evaporation. After this time, a nontransparent white bulk formed on the chip is visible. However, this is solely a dry outer shell created at the air−DNA interface that slows down water evaporation and keeps the volume within moist. Decrease of the LSPR shift for 60 and 90 mg/mL is therefore a contribution of the higher water content (smaller packing density of the DNA) at the DNA-gold interface. Several mg/mL might be the limit at which the droplet of DNA material is still able to dry within full volume at room temperature in 24 h without maintaining the residual moisture inside.

The rLSPR after each measurement is presented in Figure 3. For over 10 measurements presented, the standard deviation of the rLSPR peak was as low as σ_{rLSPR} = 2.26 nm, which highlights that our AAL and recovery protocol are reliable.

3.2. ssstDNA vs PCR DNA. We prepare a chip with AAL containing 4 structures belonging to the AchOct family and

https://doi.org/10.1021/acsomega.2c01370
ACS Omega 2022, 7, 31682−31690

with pitches of 25, 50, 100, and 263 nm. Firstly, we compare the LSPR response of AchOct 100 on two chips—the LSPR shift of 1 μg/mL ssstDNA is equal to 16 ± 5 nm in one case and 23 ± 5 nm in the other. These results prove that the AAL chip LSPR response varies from chip to chip (30% decrease in this case). We predict that factors such as time, temperature, and humidity play a role in AAL formation, and without a controlled chamber we struggled to reproduce them perfectly. By exploiting the 4-structure chip, we compare the LSPR response to the ssstDNA (heterogenous distribution ∼2000 bp) and dsDNA of homogenous distribution (546, 1064, and 1614 bp) in the 100 mM Tris and 10 mM $MgCl_2$ solution (PCR DNA).

An evolution of rLSPR in chronological order is presented in Figure 4. For 3 measurements with ssstDNA, the rLSPR peak

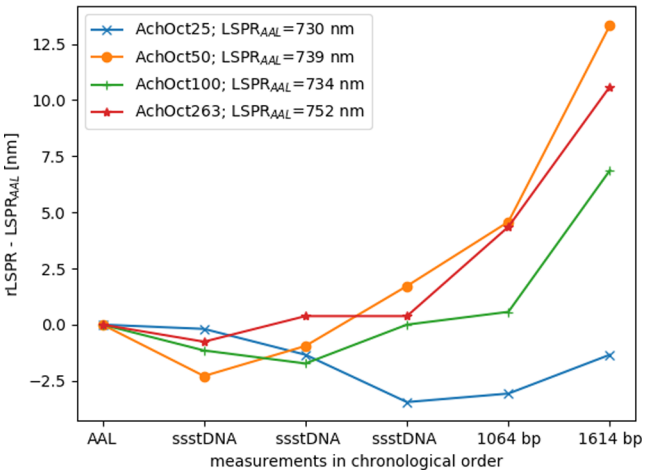

Figure 4. Evolution of the recovered LSPR (rLSPR) peak after each measurement with respect to the LSPR peak after creation of AAL (LSPR$_{AAL}$) and x-axis in chronological order. The initial LSPR peaks are provided in the legend.

stays within ±3 nm for all 4 AchOct nanostructures, which is consistent with the ±2.26 nm for AchOct 100 (Figure 3). All structures, besides AchOct 25, show a subsequent deviation from the initial LSPR after deposition of PCR DNA. Remarkably, AchOct 25 shows a good recovery of the LSPR position by staying within ±3 nm (blue curve, Figure 4), while the rest deviates more strongly from the peak position obtained with AAL (LSPR$_{AAL}$). We hypothesize a pitch-related solubility of nanocrystals of Tris and buffer created during evaporation. On the other hand, the length of the fully extended DNA composed of 500−2000 bp spans 150−600 nm. The interplay between pitch and persistence length, which is reduced when Mg^{2+} promotes condensation through charge neutralization,[23,35] could also be considered. The effect of solutes can be divided into directly on DNA, DNA−solvent, DNA−DNA interaction, and DNA−surface interaction. Factors like ion binding sites,[36] their competition,[37] and effect on local polarity,[38] conformation,[39] solvatation shell,[40] gyration radius,[41] and interactions with the surface[42] (which are all simultaneously dependent on the sequence and length[43]) are beyond the scope of this study and would have to be carefully studied.

The deviation of rLSPR from the LSPR$_{AAL}$ by over 10 nm (prior to the 546 bp measurement) may slightly alter the LSPR response for nanostructures AchOct 50 and AchOct 263. As detailed later on, their shift corresponding to 546 bp is similar to that of 1064 and 1614 bp—same as for AchOct 25 and AchOct 100. Moreover, the standard deviations of ssstDNA and PCR DNA are similar, which proves that the 546 bp measurement could not carry a significant error. Thus though not ideal, we deem the 546 bp measurement as acceptable.

The LSPR shift for ssstDNA and PCR DNA is presented in Figure 5. Starting with AchOct 25, ssstDNA gives 16 ± 4 nm

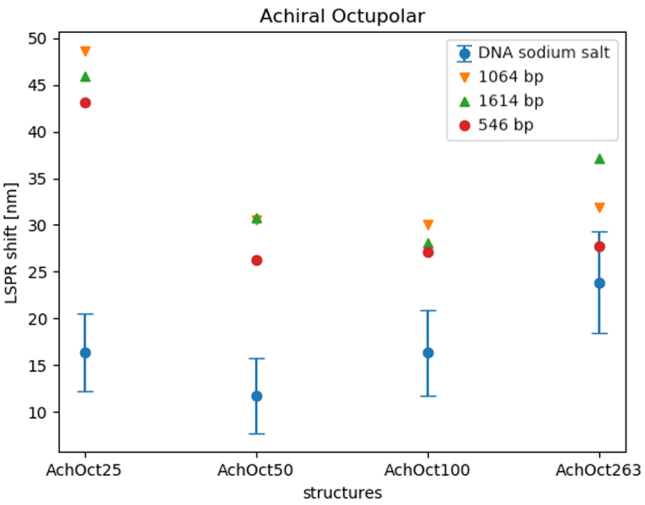

Figure 5. LSPR shift for AchOct 25/50/100/263; all samples fixed to 1 μg/mL.

(746 ± 4 nm peak position), while PCR DNA (average of 3 different molecular weights) gives 46 ± 2 nm (773 ± 1 nm peak). AchOct 50 gave 12 ± 4 nm (749 ± 3 nm peak) for ssstDNA and 29 ± 2 nm (775 ± 3 nm peak) for PCR DNA. AchOct 100 gave 16 ± 5 nm (750 ± 5 nm peak) for ssstDNA and 28 ± 1 nm (765 ± 2 nm peak) for PCR DNA. AchOct 263 gave 24 ± 5 nm (775 ± 5 nm peak) for ssstDNA and 32 ± 4 nm (789 ± 4 nm peak) for PCR DNA. Among the AchOct family, we did not find a clear indication that shorter dsDNA gives a different signal than the longer one—the standard deviation of the LSPR response of ssstDNA is comparable to that of 546/1064/1614 bp treated as 1 population (PCR DNA). Thus, we conclude that our chip LSPR response is size-independent within this molecular weight range, under the given conditions and within this standard deviation. The difference between PCR DNA and ssstDNA readings must be caused by the presence of salt and Tris in a solution. Remarkably, we found 2 structures that have the same LSPR response to ssstDNA (16 ± 4/5 nm) but differ by nearly a factor of 2 for PCR DNA (46 ± 2 and 28 ± 1 nm)—AchOct 25 and AchOct 100, respectively.

Based on our experience of working with AAL, we state that a small rLSPR is not an absolute condition for a correct measurement. Application of harsher recovery protocols allowed us to keep rLSPR within ±3 nm of LSPR$_{AAL}$, but the measurements had a much larger standard deviation—suspicion of disruption/modification of the AAL. Thus, the condition necessary for a reliable measurement is to not influence AAL rather than obtain rLSPR as close as possible to the LSPR$_{AAL}$ peak position.

Based on the preliminary results and Figure 5, we notice that increasing the pitch narrows down the difference between ssstDNA and PCR DNA. More work is required in future to

https://doi.org/10.1021/acsomega.2c01370
ACS Omega 2022, 7, 31682−31690

investigate the response for different salts. Moreover, an investigation of the nanoscale salt-triggered condensation of DNA in AAL and the deposited analyte with scanning probe techniques should be simultaneously carried out.

3.3. SERS Measurements. Measurements of surface-enhanced Raman scattering (SERS) were carried out to gather more information about AAL. In Figure 6 we present the SERS

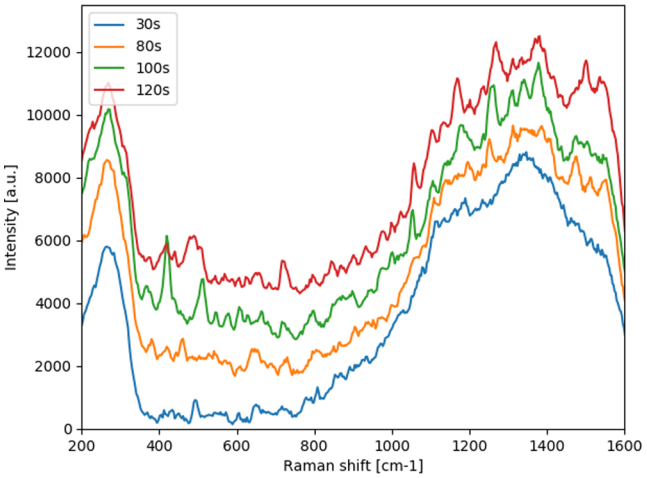

Figure 6. SERS signal collected from the DNA antiadhesive layer on the AchOct 25 structure. Offset for clarity.

signal collected from AchOct 25 with an antiadhesive DNA layer. ssstDNA gives no well-defined SERS signal until it explodes randomly and rapidly after tens of seconds of irradiation, presenting various modes and their relative intensities. This is a main obstacle in direct measurements of unmodified, long dsDNA and was already reported.[44] The observed signal evolution can be explained by the DNA melting. While Raman-active vibrations' evolution from pre- to melting DNA was described in the literature for bulk DNA,[45] we found no such relations in our SERS signal.

The random evolution of the signal in Figure 6 gives us the information that there is no particular way of ssstDNA monolayer fixation onto gold. There may be parts of DNA exposed out of the plane or free to structural changes and/or motion. Still, appearance of the signal with irradiation time indicates a clear relation with temperature and, related to it, changes in water content. The sonicated ssstDNA is severely fragmented and thus much more prone to dehydration than the long ssstDNA with its structure intact. We compare the spectra of ssstDNA, sonicated ssstDNA, and sonicated ssstDNA after acetone storage to gain insight into the hydration effect on SERS spectra.

Very carefully, we try to identify large bands to unravel the meaning of our random SERS signal. The antiadhesive layer is composed of high-molecular-weight DNA molecules that have a complex structure and hygroscopic property. Long DNA chains physiosorbed on the surface have segments adsorbed and segments exposed out of the plane of the gold surface. We compare AAL to sonicated DNA—by sonication, we expect to obtain smaller DNA fragments that would readily dehydrate and adsorb planarly with no exposed segments. Finally, by storing in acetone, we force the water loss and thermodynamically promote DNA interaction with a metallic surface.

A hydration shell is crucial for the DNA structure,[46] and it was suggested that even at 0% relative humidity up to 5−6 molecules of water per nucleotide remain.[47] Unfortunately, water bound to DNA molecules is usually calculated by using a OH stretching band above 3000 cm^{-1}, which our instruments do not cover. Many reports mention the low-frequency region (0−300 cm^{-1}) and its indirect connection to water through DNA conformation.[48−50] In our experimental spectra, a large band between 200 and 300 cm^{-1} is present in AAL (Figure 6) and sonicated dsDNA, but it decreases substantially after storage of sonicated dsDNA in acetone (Figure 7). We found

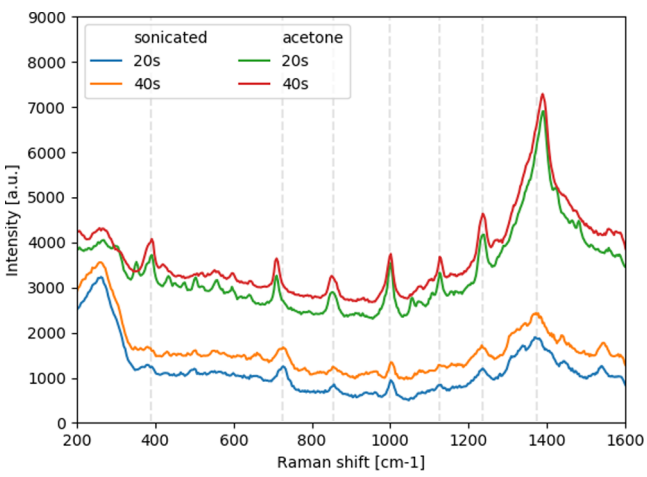

Figure 7. SERS signal collected from sonicated sodium ssstDNA (green and red) and after storing the chip in acetone for 72 h (blue and orange). Offset for clarity.

also a connection of this band to the bound water either through DNA−DNA/substrate interactions or through DNA conformation because it disappears after storing the chip in acetone. To support the claim, we look at the other peaks in the SERS spectra.

We identify 7 most prominent peaks present in both sonicated DNA and after storing in acetone, respectively: 380 and 391 cm^{-1}, 727 and 710 cm^{-1} (adenine), 853 cm^{-1} both, 1001 cm^{-1} both, 1126 cm^{-1} both, 1236 cm^{-1} both, and 1373 and 1389 cm^{-1} (adenine). If the difference between the peaks is smaller than 4 cm^{-1}, we assign them the same value due to our instrument resolution. We do not attempt to assign other vibrations than adenine—for such studies we refer the reader to experiments carried out with short poly- or single strands with known sequence.[51,52]

There are three peaks shifted by over 10 cm^{-1}. Two of them are typical peaks of adenine (727 and 1373 cm^{-1}). The latter is very sensitive to any changes, so we disregard it, but the former is reported in many studies and thus serves as a good indicator. The ring breathing mode of adenine can be found in several SERS DNA label-free studies: 732−730 cm^{-1} upon base pairing,[53] 723 cm^{-1},[5454] 735 cm^{-1},[55] and every single SERS adenine study. The peak position in different Raman experiments is as follows: powder and aqueous adenine by different teams (722 ± 4 cm^{-1};[5656] peak position for the same material can slightly vary between teams due to equipment calibration), bulk DNA melting (20 °C 729 cm^{-1} to 93 °C 725 cm^{-1}[57]), A- to B-form change (727 to 729 cm^{-1}[58]), polarization dependence in oriented fibers (731 ± 4 and 727 ± 2 cm^{-1}[59]), adenine protonation at low pH (721 ± 0 cm^{-1}[60]), and increasing Mg^{2+}/DNA till 1:5 volume ratio (727−722 cm^{-1}[61]). Note that acetone can preserve DNA for

https://doi.org/10.1021/acsomega.2c01370
ACS Omega 2022, 7, 31682−31690

years[62] or be used for DNA precipitation;[63] therefore, our 10 cm^{-1} shift cannot be caused by any chemical reaction, and the stability of DNA in acetone is indisputable. Moreover, none of the SERS and Raman studies above reported this peak below 721 cm^{-1}, regardless of the temperature, salts, and pH.

Similarly, the large shift of the ring breathing mode presented in Figure 7 (shift of 17 cm^{-1}, from 727 to 710 cm^{-1}) was observed in 3 other studies: (1) +15 cm^{-1}, from 721 to 731 cm^{-1} in TERS (chemical interaction with the tip at a tip−sample distance of 0 nm) and subsequently to 736 cm^{-1} (mechanical pressure applied by the tip−sample distance d = −1 nm),[64] (2) −15 cm^{-1} from −730 to 715 cm^{-1} upon electroplasmonic trapping of the sub-monolayer coverage of a nanourchin (ζ potential −14.6 meV) in a nanohole under 1 V bias,[65] (3) −13 cm^{-1}, from −729 to 716 cm^{-1} upon substitution of H_2O by D_2O. The third reports a similar negative shift to ours solely by a substitution of the solvent; thus, we focus on a possible solvent interaction with adenine.

Acetone is known to transfer electron to transition metal dichalcogenides;[66] if we calculate electronegativity with a formula included therein and values for gas-state species—for adenine: ionization potential (IP) = 8.3−8.5 eV[67] and electron affinity EA = −0.6−0 eV,[68] we get χ = 3.85−4.25 eV; and for acetone: IP = 9.7 eV and EA = −1.5 eV − 1.5 meV, we get χ = 4.1−4.85 eV;[69,70] gold Fermi level E_F = 5.5−5.2 eV. Direct adenine−acetone electron transfer is not likely. Substantial shift to lower frequency should cause a decrease of electron density. Studies on bound anionic states of adenine in water[71,72] indicate that the shift may be caused by acetone molecule penetration through the DNA primary hydration shell and perturbation-bound anionic state (possible withdrawal of electron density). We hypothesize that our −17 cm^{-1} shift in adenine and disappearance of the large band at 200−300 cm^{-1} indicate that even after evaporation of sonicated DNA there was plenty of bound water and loosely fixated DNA segments, and water was removed (DNA fixated) successfully by acetone storage, which brings us to the conclusion that there is plenty of bound water in AAL and it plays a crucial role by preventing both a total denaturation of DNA on the gold surface and physisorption of subsequent DNA layers onto a monolayer.

4. CONCLUSIONS

We present an e-beam-fabricated achiral octupolar plasmonic photonic crystal passivated with a novel antiadhesive DNA layer. AAL was created by immobilization of DNA sodium salt from salmon testes in a liquid-crystal concentration regime to provide optimal surface coverage. Concerning the analysis of ssstDNA in deionized water, the proposed LSPR system passivated with AAL has an LOD of 105 ng/mL, and a dynamic range up to several mg/mL was reached. AAL red-shifts the LSPR by on average 22.8 nm with respect to the bare chip, which supports the nanoscale thickness claims. However, immobilization onto different chips results in the LSPR response varying by 30%, indicating a need for a controlled chamber. Our recovery protocol is quick and requires only deionized water and acetone. It recovers perfectly after evaporation of the low-ionic-strength solution (5% NaCl/DNA content), yet its reusability is limited in case of a solution with 10 mM $MgCl_2$ and 100 mM Tris. We found no DNA size dependence on the LSPR signal within the range of 546−1614 bp based on measurements performed on the 4 nanostructures with the same achiral octupolar arrangement, but a different pitch between unit cells (25, 50, 100, and 263 nm). On the other hand, the LSPR signal was affected by the presence of the salt and buffer. Within the achiral octupolar, we identified 2 structures (AchOct 25 and AchOct 100) that for a given ssstDNA concentration return a similar LSPR shift in deionized water, while the shift for DNA in Tris buffer and magnesium salt differs by a factor of nearly 2. We collected the SERS signal to investigate the antiadhesive layer working principle and concluded that the antiadhesive property must be related to the humectant property of DNA that ensures high water content in ambient atmosphere after drying. This water layer protects the monolayer of DNA adsorbed on the gold from formation of subsequent DNA layers.

In the near future, we plan to work on the better reproducibility of antiadhesive layer sensitivity and recovery protocols for samples containing salts and buffers, and then move on to simultaneous DNA and salt concentration measurement.

■ ASSOCIATED CONTENT

Supporting Information

The Supporting Information is available free of charge at https://pubs.acs.org/doi/10.1021/acsomega.2c01370.

Electrophoresis of 546, 1064, and 1614 bp dsDNA used herein (PCR_DNA.pdf) Details on calculating the LSPR peak position and LOD (PDF)

■ AUTHOR INFORMATION

Corresponding Authors

Ambra Vestri − *Institute of Applied Sciences and Intelligent Systems "E. Caianiello" of CNR, 80072 Pozzuoli, Italy;* orcid.org/0000-0001-9877-7341; Email: ambra.vestri@isasi.cnr.it

Lucia Petti − *Institute of Applied Sciences and Intelligent Systems "E. Caianiello" of CNR, 80072 Pozzuoli, Italy;* Email: lucia.petti@isasi.cnr.it

Authors

Remigiusz K. Trojanowicz − *Advanced Materials Engineering and Modelling Group, Faculty of Chemistry, Wroclaw University of Science and Technology, 50-370 Wroclaw, Poland;* Present Address: CEA Saclay, Laboratoire d'Electronique et Photonique Organique, 91190 Gif-Sur-Yvette, France

Massimo Rippa − *Institute of Applied Sciences and Intelligent Systems "E. Caianiello" of CNR, 80072 Pozzuoli, Italy*

Joseph Zyss − *LUMIN Laboratory and Institut d'Alembert, Ecole Normale Supérieure Paris-Saclay, CNRS, Université Paris-Saclay, 91190 Gif-sur-Yvette, France*

Katarzyna Matczyszyn − *Advanced Materials Engineering and Modelling Group, Faculty of Chemistry, Wroclaw University of Science and Technology, 50-370 Wroclaw, Poland;* orcid.org/0000-0001-8578-8340

Complete contact information is available at: https://pubs.acs.org/10.1021/acsomega.2c01370

Author Contributions

‖R.K.T. and A.V. contributed equally to this work.

Notes

The authors declare no competing financial interest.

https://doi.org/10.1021/acsomega.2c01370
ACS Omega 2022, 7, 31682−31690

■ ACKNOWLEDGMENTS

The authors gratefully acknowledge support for this work from the Projects Program PNR 2015−2020 "Proof of Concept" funding the project "H2OSafety-Design and development of environmental sensors for the research of microbiological and chemical contaminants hazardous to health" (POC01_00109) and from the Project PULSE-COM (Grant agreement No 863227). This work was also supported by Erasmus+ Program which funded the collaboration with Wrocław University of Science and Technology and the Student Mobility for Traineeships Erasmus. Authors would like to thank Pierangelo Orlando and Riccardo Castagna for their help, advices and preparation of the DNA samples.

■ ABBREVIATIONS USED

AAL –antiadhesive layer; AchOct –achiral octupolar; dsDNA –double-strand DNA; PCR DNA –546, 1064, and 1614 bp in 100 mM Tris 10 mM $MgCl_2$; rLSPR –recovered LSPR peak; ssstDNA –DNA sodium salt from salmon

■ REFERENCES

(1) Liu, X.; Huang, L.; Qian, K. Nanomaterial-Based Electrochemical Sensors: Mechanism, Preparation, and Application in Biomedicine. *Adv. NanoBiomed. Res.* **2021**, *1*, No. 2000104.

(2) Moonen, E. J. M.; Haakma, J. R.; Peri, E.; Pelssers, E.; Mischi, M.; den Toonder, J. M. J. Wearable Sweat Sensing for Prolonged, Semicontinuous, and Nonobtrusive Health Monitoring. *View* **2020**, *1*, No. 20200077.

(3) Liu, J.; Cai, C.; Wang, Y.; Liu, Y.; Huang, L.; Tian, T.; Yao, Y.; Wei, J.; Chen, R.; Zhang, K.; et al. A Biomimetic Plasmonic Nanoreactor for Reliable Metabolite Detection. *Adv. Sci.* **2020**, *7*, No. 1903730.

(4) Xu, W.; Wang, L.; Zhang, R.; Sun, X.; Huang, L.; Su, H.; Wei, X.; Chen, C.-C.; Lou, J.; Dai, H.; Qian, K. Diagnosis and Prognosis of Myocardial Infarction on a Plasmonic Chip. *Nat. Commun.* **2020**, *11*, No. 1654.

(5) Szunerits, S.; Boukherroub, R. Sensing Using Localised Surface Plasmon Resonance Sensors. *Chem. Commun.* **2012**, *48*, 8999−9010.

(6) Mayer, K. M.; Hafner, J. H. Localized Surface Plasmon Resonance Sensors. *Chem. Rev.* **2011**, *111*, 3828−3857.

(7) Unser, S.; Bruzas, I.; He, J.; Sagle, L. Localized Surface Plasmon Resonance Biosensing: Current Challenges and Approaches. *Sensors* **2015**, *15*, 15684−15716.

(8) Kenausis, G. L.; Vörös, J.; Elbert, D. L.; Huang, N.; Hofer, R.; Ruiz-Taylor, L.; Textor, M.; Hubbell, J. A.; Spencer, N. D. Poly(L-Lysine)-g-Poly(Ethylene Glycol) Layers on Metal Oxide Surfaces: Attachment Mechanism and Effects of Polymer Architecture on Resistance to Protein Adsorption. *J. Phys. Chem. B* **2000**, *104*, 3298−3309.

(9) Lee, S.; Spencer, N. D. Adsorption Properties of Poly(L-Lysine)-Graft-Poly(Ethylene Glycol) (PLL-g-PEG) at a Hydrophobic Interface: Influence of Tribological Stress, PH, Salt Concentration, and Polymer Molecular Weight. *Langmuir* **2008**, *24*, 9479−9488.

(10) Liu, J. Adsorption of DNA onto Gold Nanoparticles and Graphene Oxide: Surface Science and Applications. *Phys. Chem. Chem. Phys.* **2012**, *14*, 10485−10496.

(11) Koo, K. M.; Sina, A. A. I.; Carrascosa, L. G.; Shiddiky, M. J. A.; Trau, M. DNA-Bare Gold Affinity Interactions: Mechanism and Applications in Biosensing. *Anal. Methods* **2015**, *7*, 7042−7054.

(12) Chen, D.; Zhou, J.; Rippa, M.; Petti, L. Structure-Dependent Localized Surface Plasmon Resonance Characteristics and Surface Enhanced Raman Scattering Performances of Quasi-Periodic Nanoarrays: Measurements and Analysis. *J. Appl. Phys.* **2015**, *118*, No. 163101.

(13) Jo, N. rae.; Shin, Y. B. Enhancing Biosensing Sensitivity of Metal Nanostructures through Site-Selective Binding. *Sci. Rep.* **2020**, *10*, No. 1024.

(14) Aćimović, S. S.; Šípová, H.; Emilsson, G.; Dahlin, A. B.; Antosiewicz, T. J.; Käll, M. Superior LSPR Substrates Based on Electromagnetic Decoupling for On-a-Chip High-Throughput Label-Free Biosensing. *Light: Sci. Appl.* **2017**, *6*, No. e17042.

(15) Balamurugan, S.; Mayer, K. M.; Lee, S.; Soper, S. A.; Hafner, J. H.; Spivak, D. A. Nanostructure Shape Effects on Response of Plasmonic Aptamer Sensors. *J. Mol. Recognit.* **2013**, *26*, 402−407.

(16) Rippa, M.; Castagna, R.; Pannico, M.; Musto, P.; Tkachenko, V.; Zhou, J.; Petti, L. Engineered Plasmonic Thue-Morse Nanostructures for LSPR Detection of the Pesticide Thiram. *Nanophotonics* **2017**, *6*, 1083−1092.

(17) Rippa, M.; Castagna, R.; Tkachenko, V.; Zhou, J.; Petti, L. Engineered Nanopatterned Substrates for High-Sensitive Localized Surface Plasmon Resonance: An Assay on Biomacromolecules. *J. Mater. Chem. B* **2017**, *5*, 5473−5478.

(18) Vestri, A.; Rippa, M.; Marchesano, V.; Sagnelli, D.; Margheri, G.; Zhou, J.; Petti, L. LSPR Immuno-Sensing Based on Iso-Y Nanopillars for Highly Sensitive and Specific Imidacloprid Detection. *J. Mater. Chem. B* **2021**, *9*, 9153−9161.

(19) Rippa, M.; Castagna, R.; Brandi, S.; Fusco, G.; Monini, M.; Chen, D.; Zhou, J.; Zyss, J.; Petti, L. Octupolar Plasmonic Nanosensor Based on Ordered Arrays of Triangular Au Nanopillars for Selective Rotavirus Detection. *ACS Appl. Nano Mater.* **2020**, *3*, 4837−4844.

(20) Palermo, G.; Rippa, M.; Conti, Y.; Vestri, A.; Castagna, R.; Fusco, G.; Suffredini, E.; Zhou, J.; Zyss, J.; De Luca, A.; Petti, L. Plasmonic Metasurfaces Based on Pyramidal Nanoholes for High-Efficiency SERS Biosensing. *ACS Appl. Mater. Interfaces* **2021**, *13*, 43715−43725.

(21) Zyss, J. Molecular Engineering Implications of Rotational Invariance in Quadratic Nonlinear Optics: From Dipolar to Octupolar Molecules and Materials. *J. Chem. Phys.* **1993**, *98*, 6583−6599.

(22) Rippa, M.; Castagna, R.; Pannico, M.; Musto, P.; Borriello, G.; Paradiso, R.; Galiero, G.; Bolletti Censi, S.; Censi, S. B.; Zhou, J.; Zyss, J. Octupolar Metastructures for a Highly Sensitive, Rapid, and Reproducible Phage-Based Detection of Bacterial Pathogens by Surface-Enhanced Raman Scattering. *ACS Sens.* **2017**, *2*, 947−954.

(23) Guilbaud, S.; Salomé, L.; Destainville, N.; Manghi, M.; Tardin, C. Dependence of DNA Persistence Length on Ionic Strength and Ion Type. *Phys. Rev. Lett.* **2019**, *122*, No. 028102.

(24) Robertson, R. M.; Laib, S.; Smith, D. E. Diffusion of Isolated DNA Molecules: Dependence on Length and Topology. *Proc. Natl. Acad. Sci. U.S.A.* **2006**, *103*, 7310−7314.

(25) García-Alegría, A. M.; Anduro-Corona, I.; Pérez-Martínez, C. J.; Corella-Madueño, M. A. G.; Rascón-Durán, M. L.; Astiazaran-Garcia, H. Quantification of DNA through the Nanodrop Spectrophotometer: Methodological Validation Using Standard Reference Material and Sprague Dawley Rat and Human DNA. *Int. J. Anal. Chem.* **2020**, *2020*, No. 8896738.

(26) Bruijns, B. B.; Tiggelaar, R. M.; Gardeniers, J. G. E. Fluorescent Cyanine Dyes for the Quantification of Low Amounts of DsDNA. *Anal. Biochem.* **2016**, *511*, 74−79.

(27) Kawasaki, D.; Yamada, H.; Maeno, K.; Sueyoshi, K.; Hisamoto, H.; Endo, T. Core−Shell-Structured Gold Nanocone Array for Label-Free DNA Sensing. *ACS Appl. Nano Mater.* **2019**, *2*, 4983−4990.

(28) Tanaka, K.; Okahata, Y. A DNA-Lipid Complex in Organic Media and Formation of an Aligned Cast Film. *J. Am. Chem. Soc.* **1996**, *118*, 10679−10683.

(29) Zyss, J.; Brasselet, S.; Thalladi, V. R.; Desiraju, G. R. Octupolar versus Dipolar Crystalline Structures for Nonlinear Optics: A Dual Crystal and Propagative Engineering Approach. *J. Chem. Phys.* **1998**, *109*, 658−669.

(30) Thermo Fisher Scientific. NanoDrop 2000/2000c Spectrophotometer.

(31) Olesiak, J.; Matczyszyn, K.; Mojzisova, H.; Zlelinski, M.; Chauvat, D.; Zyss, J. Liquid Crystalline Phases in DNA and Dye-

https://doi.org/10.1021/acsomega.2c01370
ACS Omega 2022, 7, 31682−31690

Doped DNA Solutions Analysed by Polarized Linear and Nonlinear Microscopy and Differential Scanning Calorimetry. *Mater. Sci. Pol.* **2009**, *27*, 813−823.
(32) Strzelecka, T. E.; Davidson, M. W.; Rill, R. L. Multiple Liquid Crystal Phases of DNA at High Concentrations. *Nature* **1988**, *331*, 457−460.
(33) Russell, K. J.; Yeung, K. Y. M.; Hu, E. Measuring the Mode Volume of Plasmonic Nanocavities Using Coupled Optical Emitters. *Phys. Rev. B: Condens. Matter Mater. Phys.* **2012**, *85*, No. 245445.
(34) Kaminska, I.; Maurer, T.; Nicolas, R.; Renault, M.; Lerond, T.; Salas-Montiel, R.; Herro, Z.; Kazan, M.; Niedziolka-Jönsson, J.; Plain, J.; et al. Near-Field and Far-Field Sensitivities of LSPR Sensors. *J. Phys. Chem. C* **2015**, *119*, 9470−9476.
(35) Bloomfield, V. A. DNA Condensation by Multivalent Cations. *Biopolymers* **1997**, *44*, 269−282.
(36) Leonarski, F.; D'Ascenzo, L.; Auffinger, P. Mg2+ Ions: Do They Bind to Nucleobase Nitrogens? *Nucleic Acids Res.* **2017**, *45*, 987−1004.
(37) Xi, K.; Wang, F. H.; Xiong, G.; Zhang, Z. L.; Tan, Z. J. Competitive Binding of Mg2+ and Na+ Ions to Nucleic Acids: From Helices to Tertiary Structures. *Biophys. J.* **2018**, *114*, 1776−1790.
(38) Jadhav, V. R.; Barawkar, D. A.; Ganesh, K. N. Polarity Sensing by Fluorescent Oligonucleotides: First Demonstration of Sequence-Dependent Microenvironmental Changes in the DNA Major Groove. *J. Phys. Chem. B* **1999**, *103*, 7383−7385.
(39) Tan, Z. J.; Chen, S. J. Nucleic Acid Helix Stability: Effects of Salt Concentration, Cation Valence and Size, and Chain Length. *Biophys. J.* **2006**, *90*, 1175−1190.
(40) Feig, M.; Pettitt, B. M. Sodium and Chlorine Ions as Part of the DNA Solvation Shell. *Biophys. J.* **1999**, *77*, 1769−1781.
(41) Sim, A. Y. L.; Lipfert, J.; Herschlag, D.; Doniach, S. Salt Dependence of the Radius of Gyration and Flexibility of Single-Stranded DNA in Solution Probed by Small-Angle x-Ray Scattering. *Phys. Rev. E: Stat., Nonlinear, Soft Matter Phys.* **2012**, *86*, No. 021901.
(42) Erdmann, M.; David, R.; Fornof, A. R.; Gaub, H. E. Electrically Induced Bonding of DNA to Gold. *Nat. Chem.* **2010**, *2*, 745−749.
(43) Svozil, D.; Kalina, J.; Omelka, M.; Schneider, B. DNA Conformations and Their Sequence Preferences. *Nucleic Acids Res.* **2008**, *36*, 3690−3706.
(44) Barhoumi, A.; Zhang, D.; Tam, F.; Halas, N. J. Surface-Enhanced Raman Spectroscopy of DNA. *J. Am. Chem. Soc.* **2008**, *130*, 5523−5529.
(45) Erfurth, S. C.; Peticolas, W. L. Melting and Premelting Phenomenon in DNA by Laser Raman Scattering. *Biopolymers* **1975**, *14*, 247−264.
(46) Tao, N. J. Light Scattering Spectroscopy Studies of the Water Molecules in DNA. In *Water and Biological Macromolecules. Topics in Molecular and Structural Biology*, Palgrave, 1993; pp 266−292.
(47) Tao, N. J.; Lindsay, S. M.; Rupprecht, A. Structure of DNA Hydration Shells Studied by Raman Spectroscopy. *Biopolymers* **1989**, *28*, 1019−1030.
(48) Thomas, G. J. Water as a Bioactivator and Probe of DNA Structure: Investigation by Laser Raman Spectroscopy. In *Spectroscopy of Inorganic Bioactivators*, Springer, 1989; pp 247−263.
(49) Lamba, O. P.; Wang, A. H.; Thomas, G. J. Low-frequency Dynamics and Raman Scattering of Crystals, of B-, A-, and Z-DNA, and Fibers of C-DNA. *Biopolymers* **1989**, *28*, 667−678.
(50) Weidlich, T.; Lindsay, S. M.; Ruil, Q.; Rupprecht, A.; Peticolas, W. L.; Thomas, G. A. A Raman Study of Low Frequency Intrahelical Modes in A-, b-, and c-Dna. *J. Biomol. Struct. Dyn.* **1990**, *8*, 139−171.
(51) Garcia-Rico, E.; Alvarez-Puebla, R. A.; Guerrini, L. Direct Surface-Enhanced Raman Scattering (SERS) Spectroscopy of Nucleic Acids: From Fundamental Studies to Real-Life Applications. *Chem. Soc. Rev.* **2018**, *47*, 4909−4923.
(52) Pyrak, E.; Krajczewski, J.; Kowalik, A.; Kudelski, A.; Jaworska, A. Surface Enhanced Raman Spectroscopy for DNA Biosensors - How Far Are We? *Molecules* **2019**, *24*, No. 4423.
(53) Li, Y.; Gao, T.; Xu, G.; Xiang, X.; Zhao, B.; Han, X. X.; Guo, X. Direct Approach toward Label-Free DNA Detection by Surface-Enhanced Raman Spectroscopy: Discrimination of a Single-Base Mutation in 50 Base-Paired Double Helixes. *Anal. Chem.* **2019**, *91*, 7980−7984.
(54) Xu, L. J.; Lei, Z. C.; Li, J.; Zong, C.; Yang, C. J.; Ren, B. Label-Free Surface-Enhanced Raman Spectroscopy Detection of DNA with Single-Base Sensitivity. *J. Am. Chem. Soc.* **2015**, *137*, 5149−5154.
(55) Lin, D.; Wu, Q.; Qiu, S.; Chen, G.; Feng, S.; Chen, R.; Zeng, H. Label-Free Liquid Biopsy Based on Blood Circulating DNA Detection Using SERS-Based Nanotechnology for Nasopharyngeal Cancer Screening. *Nanomedicine Nanotechnology, Biol. Med.* **2019**, *22*, No. 102100.
(56) Nergui, N.; Chen, M. J.; Wang, J. K.; Wang, Y. L.; Hsing, C. R.; Wei, C. M.; Takahashi, K. Dependence of Adenine Raman Spectrum on Excitation Laser Wavelength: Comparison between Experiment and Theoretical Simulations. *J. Phys. Chem. A* **2016**, *120*, 8114−8122.
(57) Duguid, J. G.; Bloomfield, V. A.; Benevides, J. M.; Thomas, G. J. DNA Melting Investigated by Differential Scanning Calorimetry and Raman Spectroscopy. *Biophys. J.* **1996**, *71*, 3350−3360.
(58) Gorelik, V. S.; Krylov, A. S.; Sverbil, V. P. Local Raman Spectroscopy of DNA. *Bull. Lebedev Phys. Inst.* **2014**, *41*, 310−315.
(59) Thomas, G. J.; Benevides, J. M.; Overman, S. A.; Ueda, T.; Ushizawa, K.; Saitoh, M.; Tsuboi, M. Polarized Raman Spectra of Oriented Fibers of A DNA and B DNA: Anisotropic and Isotropic Local Raman Tensors of Base and Backbone Vibrations. *Biophys. J.* **1995**, *68*, 1073−1088.
(60) O'Connor, T.; Mansy, S.; Bina, M.; McMillin, D. R.; Bruck, M. A.; Tobias, R. S. The PH-Dependent Structure of Calf Thymus DNA Studied by Raman Spectroscopy. *Biophys. Chem.* **1982**, *15*, 53−64.
(61) M. Structural Analysis of DNA Interactions with Magnesium Ion Studied by Raman Spectroscopy. *Am. J. Biochem. Biotechnol.* **2011**, *7*, 135−140.
(62) Fukatsu, T. Acetone Preservation: A Practical Technique for Molecular Analysis. *Mol. Ecol.* **1999**, *8*, 1935−1945.
(63) Bryzgunova, O.; Bondar, A.; Morozkin, E.; Mileyko, V.; Vlassov, V.; Laktionov, P. A Reliable Method to Concentrate Circulating DNA. *Anal. Biochem.* **2011**, *408*, 354−356.
(64) Ichimura, T.; Fujii, S.; Verma, P.; Yano, T.; Inouye, Y.; Kawata, S. Subnanometric Near-Field Raman Investigation in the Vicinity of a Metallic Nanostructure. *Phys. Rev. Lett.* **2009**, *102*, No. 186101.
(65) Huang, J. A.; Mousavi, M. Z.; Zhao, Y.; Hubarevich, A.; Omeis, F.; Giovannini, G.; Schütte, M.; Garoli, D.; De Angelis, F. SERS Discrimination of Single DNA Bases in Single Oligonucleotides by Electro-Plasmonic Trapping. *Nat. Commun.* **2019**, *10*, No. 5321.
(66) Choi, J.; Zhang, H.; Du, H.; Choi, J. H. Understanding Solvent Effects on the Properties of Two-Dimensional Transition Metal Dichalcogenides. *ACS Appl. Mater. Interfaces* **2016**, *8*, 8864−8869.
(67) Roca-Sanjuán, D.; Rubio, M.; Merchán, M.; Serrano-Andrés, L. Ab Initio Determination of the Ionization Potentials of DNA and RNA Nucleobases. *J. Chem. Phys.* **2006**, *125*, No. 084302.
(68) Wesolowski, S. S.; Leininger, M. L.; Pentchev, P. N.; Schaefer, H. F. Electron Affinities of the DNA and RNA Bases. *J. Am. Chem. Soc.* **2001**, *123*, 4023−4028.
(69) Vera, D. M. A.; Pierini, A. B. Species with Negative Electron Affinity and Standard DFT Methods. *Phys. Chem. Chem. Phys.* **2004**, *6*, 2899−2903.
(70) NIST chemistry WebBook. http://webbook.nist.gov/chemistry (accessed Jul 22, 2021).
(71) Harańczyk, M.; Gutowski, M.; Li, X.; Bowen, K. H. Bound Anionic States of Adenine. *Proc. Natl. Acad. Sci. U. S. A.* **2007**, *104*, 4804−4807.
(72) Jalbout, A. F.; Adamowicz, L. Dipole-Bound Anions of Adenine-Water Clusters. Ab Initio Study. *J. Phys. Chem. A* **2001**, *105*, 1033−1038.

https://doi.org/10.1021/acsomega.2c01370
ACS Omega 2022, 7, 31682−31690